УДК 542.9:544.01

James T. A. JONES[1], Paul V. WIPER[1] and Yaroslav Z. KHIMYAK[1,2]

INCORPORATION OF ALUMINIUM INTO –CH_2CH_2–/–CH=CH–PMOS

[1]University of Liverpool
Liverpool, L69 7ZD, United Kingdom

[2]University of East Anglia
Norwich Research Park, Norwich NR4 7TJ
e-mail: Y.Khimyak@uea.ac.uk

A series of multi-component aluminium containing –CH_2CH_2–/–CH=CH– periodic mesoporous organosilica (PMO) has been prepared via cationic templating. The influence of pre-hydrolysis on the distribution of the organic and inorganic moieties has been investigated using a variety of complementary solid-state NMR techniques.

Keywords: aluminium, mesoporous organosilica.

Introduction

Materials combining a uniform mix of organic functionalities imbedded covalently in the pore walls of an inorganic matrix are referred to as periodic mesoporous organosilicas (PMOs). Their discovery in 1999 exploited methods used previously for MCM/SBA synthesis [1, 2]. However the precursor, being a bridged organo-silsequioxane (($R'O)_3$–Si–R–Si$(OR')_3$)) where R = Me/Et/Ar etc. ensured direct inclusion of covalent Si–C bonds via hydrolysis and condensation using a suitable acid/base catalyst [3, 4]. In comparison with their inorganic counterparts, PMOs possess several advantages: replacing hydrophilic Si–OH with Si–R groups increases the hydrophobicity, mechanical strength and hydrothermal stability [5, 6]. Si–O–Si and pendant Si–OR groups are easily hydrolysed, whereas Si–C (sp3) bonds are much more resistant, resulting in greater stability. High loadings of organic content are possible with insignificant pore blocking, which can be further utilised to anchor or graft various functional groups [7, 8].

Heteroatoms have been incorporated into purely inorganic mesostructured materials for tailoring of their catalytic properties. However, only few examples have been reported for PMOs. Typically, heteroatom functionalisation can be achieved *via* isomorphous substitution of silicon atoms for an appropriate metal atom [9]. To date, heteroatoms such as, Aluminium, Titanium, Vanadium and Chromium have been introduced into mono-functional PMOs. Aluminium/ethane synthesised PMOs were independently reported by Hughes and Guo *et al.* [10, 11] by a direct synthetic method with the use of cationic surfactants under basic conditions (S^+I) [12]. The incorporation of aluminium into organosilica frameworks yielded bridging hydroxyls (≡Si–OH–Al≡)

which was confirmed using pyridine adsorption and subsequent FTIR measurements. These materials are promising as acid catalysts with the opportunity for greater control of hydrophilic/hydrophobic properties. They may also subsequently replace Al-MCM-41 to be employed as an acid catalyst for the alkylation of hydrocarbons. Cho [13] and Inagaki [14] *et al.* reported the use of titanium/ethane PMOs for photocatalytic reactions. Shylesh et al. [15] demonstrated the successful synthesis of chromium containing PMOs *via* direct co-condensation of BTSE and TEOS with chromium nitrate. The catalytic activity of converting cyclohexane to cyclohexanone and cyclohexanol, (both are intermediates in producing adipic acid (Nylon-6,6) and caprolactam (Nyclon-6)) over Cr–PMOs in the presence of H_2O_2 was tested. Successful conversions of up to 33 and 62 % for cyclohexanone and cyclohexanol respectively were reported, indicating an effective oxidation catalyst. Shylesh et al. [16] also reported the first vanadium containing PMOs as a potential catalyst in epoxidation reactions of styrene. V–PMOs exhibited higher catalytic activity to their V–MCM counterparts. However, none of the mentioned publications provided any information on the location of heteroatoms in the framework. The distribution of the active sites has a pronounced effect on overall catalytic activity of porous solids.

Solid-state NMR is a non-destructive spectroscopic tool that is used to characterise amorphous materials on the molecular level [17–19]. Typically, 1D NMR techniques such as ^{1}H MAS, ^{1}H-^{29}Si, ^{13}C cross-polarisation under magic-angle spinning (CP-MAS) are used to confirm the incorporation of organic groups and retention of Si–C bonds [20]. CP kinetics and two-dimensional (2D) NMR experiments provide information on molecular dynamics, mobilities and spatial proximities of different components of the framewrok [21]. We reported the synthesis of well-ordered $–CH_2–CH_2–$/–CH=CH– PMOs with controlled heterogeneous domains using a novel pre-hydrolysis step [22]. Herein we present the synthesis of aluminium containing $–CH_2CH_2$/–CH=CH–PMOs using cationic templating under basic conditions. ^{1}H-^{29}Si, ^{1}H-^{27}Al heteronuclear correlation (HECTOR) and ^{1}H-^{29}Si CP kinetics experiments were used to probe the influence of a joint or separate pre-hydrolysis step during synthesis on the distribution of organic functionalities and aluminium in the porous framework. The ability to design such complex solids could have particular use in chromatographic, catalytic and controlled release applications.

Experimental details

Synthesis. All starting materials were used as received without further purification: organosilane precursors, 1,2-bis(triethoxysilyl)ethylene (BTSEY 80% trans isomer, 95%, Gelest), 1,2-bis(triethoxysilyl)ethane (BTSE, 99%, Aldrich), Octadecyltrimethyl-ammonium Bromide (ODTABr, 98%, Aldrich), Aluminium isopropoxide ($Ali(OC_3H_7)_3$, 98%, Aldrich), sodium chloride (NaCl), sodium hydroxide (NaOH, 98%) all from Aldrich.

In a typical synthesis Octadecyltrimethyl ammonium Bromide (0.633 g) was dissolved in DDI water (11.36 ml) and 1M NaOH (6.71 ml) at 40 °C. When the solution became homogenous a mixture of BTSE (0.526 ml), BTSEY (0.524 ml), Aluminium iso-propoxide (0.058 g) and ethanol (1.2 ml) were added and stirred at 40°C for 24 hours. The resulting white suspension was placed in the oven at 95°C for 4 days. The solid products were recovered by vacuum filtration after cooling to ambient temperature. The final product was washed sequentially with deionised water and ethanol, and dried at ca. 70 °C. The final molar composition of synthesis mixture was 0.5 BTSE: 0.5 BTSEY:

0.56 ODTABr: 347.6 H_2O: 2 NaOH: 0.1 Al_{ISO}. The template was removed by solvent extraction. Typically, *ca*. 0.5 g of as-synthesised solid was added to 50 ml of 18.8×10^{-3}M HCl/EtOH and stirred for 4 hours at 50°C [11]. The resulting white product was cooled to room temperature, vacuum filtered and dried at 100°C. The process was repeated three times to ensure efficient template removal. Bi-functional –CH_2CH_2–/–CH=CH–PMOs were synthesised using the same procedure with the omission of the Al source and the template extraction procedure used a 1M HCl/EtOH solution as described above.

The organosilane and aluminium precursor pre-hydrolysis was also used to test the distribution of aluminium within the mesoporous framework. The Si/NaOH ratio was 14.1 along with the Si/EtOH = 0.18 (Table 1). Joint pre-hydrolysis involved combining all 3 precursors (BTSE, BTSEY and $Al(^iOC_7H_5)_3$) in a solution of EtOH/NaOH and stirring at room temperature for 30 or 60 minutes prior to the addition to the solution of the template. The separate pre-hydrolysis conditions involved combining the aluminium precursor with either BTSE or BTSEY in one vial and the pristine silicon precursor in another. After 30 or 60 minutes both reaction mixtures are stirred into the template solution. The final molar gel composition was kept constant irrespectively of pre-hydrolysis conditions. Two reference PMOs prepared without pre-hydrolysis are labelled as follows; Al–CH_2CH_2–/–CH=CH–PMO corresponding to a tri-functional PMO with Si/Al = 5 and CH_2CH_2–/–CH=CH–PMO corresponding to a bifunctional PMO synthesized in the absence of aluminium.

Table 1

Summary of pre-hydrolysis conditions and their corresponding sample names

Sample[a]	Si/Al ratio	Pre-hydrolysis time / (min)
J-PMO-5-30	5	30
J-PMO-5-60	5	60
S-PMO-5-30-EAl	5	30
S-PMO-5-60-EAl	5	60
S-PMO-5-30-YAl	5	30
S-PMO-5-60-YAl	5	60

[a]E and Y denote -CH2CH2- and -CHCH- precursor pre-hydrolysed with Al.

Characterisation

Powder X-ray diffraction (PXRD) patterns were measured using a Panalytical X-pert pro diffractometer with Co-$K_{\alpha1}$ radiation with a wavelength λ = 1.789 Å. Patterns were recorded in Bragg-Brentano geometry and measured in the 1.2 – 8° 2θ range, using a flat sample holder.

Nitrogen adsorption-desorption isotherms were measured on a Micromeritics ASAP2420 system at –196°C. The samples were dried and evacuated for 5 hours at 120 °C before analysis. The specific surface area was calculated using BET method using linear plot over a range of p/p_o = 0.06–0.20. The pore size distribution was calculated using the adsorption branch of the isotherm using Barrett-Joyner-Halenda (BJH) method. Pore volume was calculated from the amount of adsorbed nitrogen at p/p_o = 0.99. Micropore volume and surface areas were obtained from the t-plot method using Harkins-Jura reference isotherm ($t = (13.99/(0.034 - \log p/p_s))^{1/2}$).

Solid-state NMR experiments were conducted at 9.4 T using a Bruker DSX400 spectrometer operating at 79.49, 100.61, 104.26 and 400.13 MHz for ^{29}Si, ^{13}C, ^{27}Al and ^{1}H respectively. ^{29}Si, ^{13}C and ^{1}H chemical shifts are quoted in ppm from external TMS.

^{27}Al chemical shifts are quoted in ppm from 1M $[Al(H_2O)_6]^{3+}$. Samples were spun in zirconia rotors driven by N_2 gas using either a 4 mm $^{1}H/X/Y$ or 2.5 mm $^{1}H/^{19}F/X$ commercial probeheads.

^{1}H-^{13}C CP/MAS NMR spectra were acquired at an MAS rate of 8.0 kHz. A ^{1}H $\pi/2$ pulse length was 3.0 μs and the recycle delay was 8.0 s. The CP contact time was 1.0 ms with the Hartman–Hahn matching condition set using Hexamethylbenzene (HMB). ^{1}H-^{13}C CP/MAS kinetics spectra were acquired using contact times in the range of 0.01 to 16.0 ms.

^{1}H-^{29}Si CP/MAS NMR spectra were acquired at an MAS rate of 4.0 kHz. A ^{1}H $\pi/2$ pulse length of 3.1 μs and the recycle delay of 10 s was used during acquisition. The CP contact time was 6.0 ms with the Hartmann–Hahn matching condition set using kaolinite. The ^{1}H-^{29}Si CP kinetics measurements used contact times ranging from 0.05 to 16.0 ms.

^{27}Al MAS NMR spectra were acquired using a ^{27}Al $\pi/10$ pulse length of 0.4 μs at a MAS rate of 10.0 kHz and a recycle delay of 1.0 s. All ^{27}Al MAS NMR spectra were acquired using the same 2048 scans to obtain quantitative information for different samples.

^{1}H-^{27}Al CP/MAS NMR spectra were acquired at an MAS rate of 10 kHz. The ^{1}H $\pi/2$ pulse length was 2.8 μs and the recycle delay was 5.0 s. The CP contact time was 2.0 ms with the Hartman-Hahn matching condition set using gibbsite.

2D ^{1}H-^{29}Si Heteronuclear correlation (HETCOR) MAS NMR spectra were acquired at an MAS rate of 10 kHz. The 2D HETCOR experiments used Frequency-Switched Lee-Goldburg (FSLG) homonuclear decoupling with ^{1}H *rf* field of ca. 80.6 kHz in t_1 and ramp-amplitude ^{1}H-^{29}Si cross-polarization with a contact time of 2.0 ms. TPPM decoupling was used during acquisition at a decoupling strength of *ca.* 80.6 kHz. The sample volume was restricted to the middle of the rotor to improve the *rf* homogeneity. States-TPPI was employed for phase sensitive detection [23, 24]. The recycle delay was set at 2.0 s. 256 increments were recorded in t_1 to cover the full ^{1}H spectral width of 23048 Hz corresponding to a dwell time of 43.4 μs. 600 scans acquired in t_2 per increment.

2D ^{1}H-^{27}Al HETCOR MAS NMR spectra were acquired at an MAS rate of 10 kHz. The FSLG homonuclear decoupling with a ^{1}H *rf* field of approximately 80.6 kHz in t_1 and ramp amplitude ^{1}H-^{27}Al CP with a contact time of 2.0 ms were used. TPPM decoupling was applied during acquisition at a decoupling strength of *ca.* 80.6 kHz. The sample volume was restricted to the middle of the rotor to improve the rf homogeneity. States-TPPI was employed for phase sensitive detection. The recycle delay was set at 1.5 s. 256 increments were recorded in t_1 to cover the full ^{1}H spectral width of 23048 Hz corresponding to a dwell time of 43.4 μs. 800 scans acquired in t_2 per increment.

Results and Discussion

Mesoscopic ordering of Al-PMOs

PXRD patterns of the template extracted reference PMOs (Fig. 1) confirm the presence of a 2D hexagonal mesostructure with d_{100} spacings of 49.0 Å for $–CH_2CH_2–$/ –CH=CH–PMO and 42.7 Å for Al/$–CH_2CH_2–$/–CH=CH–PMO. The reduction of the unit cell upon incorporation of aluminium is coupled with improved mesoscopic ordering, indicated by more intense (110) and (200) reflections compared to the Al-free PMO. A possible rationale for this observation lies in the generation of negatively

charged framework by isomorphous substitution of Si^{4+} for Al^{3+}, balanced by either an acidic proton or counter cation. As these PMOs are synthesised via the S^+I^- pathway (S^+ represents the cationic surfactant head group and I^- the negatively charged silicate species), the self-assembly relies on the electrostatic interaction between S^+ and I^-. The generation of negative framework sites for aluminium-containing PMOs would, therefore, induce a greater template/framework electrostatic interaction. A steady increase in mesoscopic ordering in a series Si/Al = 20, 10 and 5 corroborates this hypothesis and is in agreement with reported Al–/–CH_2CH_2–PMOs. The powder XRD patterns of the template-extracted pre-hydrolysed PMOs (Fig. 2) all display d_{100} spacings of *ca.* 44 Å, similar to the standard Al–CH_2CH_2–/–CH=CH–PMO. The degree of mesoscopic ordering is reduced in all the pre-hydrolysed samples (with the exception of J-PMO-5-30 and S-PMO-5-30 (–CH=CH– + Al) which show patterns similar to the standard Al/–CH_2CH_2–/–CH=CH–PMO).

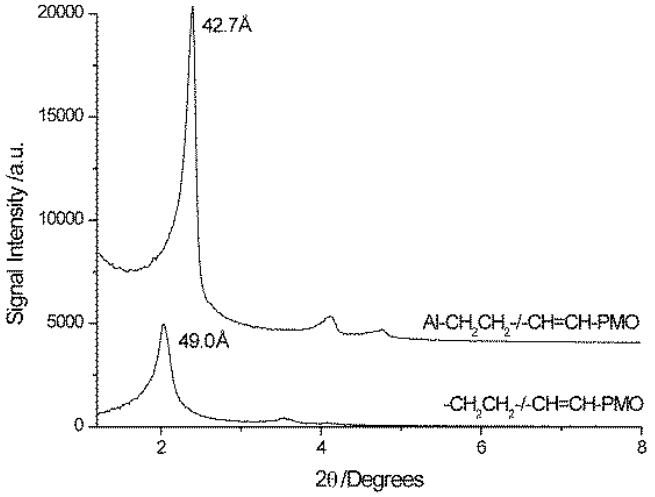

Fig. 1. PXRD patterns of the reference PMOs after template extraction.

The pre-hydrolysis of $Al(O^iC_3H_7)_3$ and alkyl silicon alkoxides in H_2O/OH- media would lead to negatively charged clusters. Such clusters would also be bulky and might cause electrostatic repulsion between one another. This will reduce the efficiency of co-assembly with the template micelles and, hence, could lead to a reduction in mesoscopic ordering, confirmed by PXRD. However, the high degree of mesoscopic ordering seen for J-PMO-5-30 and S-PMO-5-30-Y/Al suggests that pre-hydrolysis and the formation of SBUs before addition to the template are not the only factor to consider. Other parameters such as, the efficiency of aluminium incorporation and –CH_2CH_2–/–CH=CH– ratio do not show any coherent correlation (albeit based on limited number of tried Al/–CH_2–CH_2–/CH=CH– ratios and experimental protocols) between mesoscopic ordering and Al content or increasing CH_2CH_2–/–CH=CH– ratios. Under alkaline conditions, the hydrolysis of metal alkoxides produces strong nucleophiles via the deprotonation of hydroxyl groups. Rapid co-condensation occurs forming T–O–T–O–T (T = Si/Al) SBUs.

The formation of ordered composites relies on the ability for these SBUs to assemble around template aggregates. Smaller, more reactive SBUs are likely to undergo a more efficient assembly with template compared to larger units. In pre-hydrolysised systems, a low base content (Si/NaOH = 14.1) favours the formation of highly ordered PMOs compared to solids obtained using a high base content (Si/NaOH = 2.6) which gave disordered products. However, this appears to be a specific feature for the Al–/–CH_2CH_2–/–CH=CH–PMOs as –CH_2CH_2–/–CH=CH–[22] and CH_2CH_2–/–C_6H_4–PMOs[25] still formed ordered arrays under these conditions.

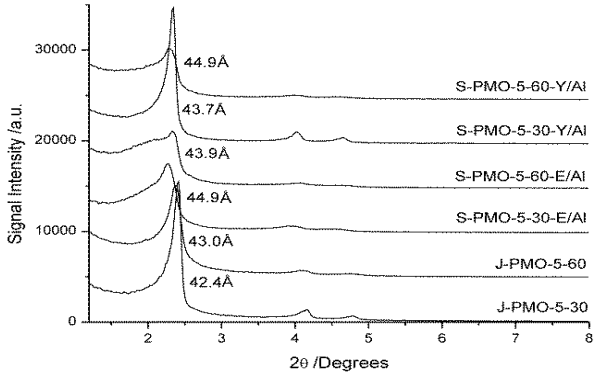

Fig. 2. PXRD patterns of the pre-hydrolysed Al containing –CH_2CH_2–/–CH=CH–PMOs after template extraction.

N_2 adsorption-desorption isotherms were used to monitor the effects of incorporation of aluminium and pre-hydrolysis on the textural properties of the resulting PMOs. Both the reference PMOs display type IV isotherms confirming their mesoporous structure (Fig. 2, left). A broad capillary condensation step is observed in the region of p/p_o = 0.4 to 0.6 for both samples. Upon desorption a change in hysteresis from a Type H1 to H3 coupled with a second maximum in the PSD plot at ca. 128 Å, suggest the presence of inter-particle porosity, is observed upon Al incorporation. The N_2 adsorption-desorption isotherms of the pre-hydrolysed PMOs (Fig. 3 middle and right) also show type IV isotherms but the capillary condensation step is less well defined indicating a less uniform porous structure. The isotherm of S-PMO-5-60-Y/Al resembles a type II isotherm confirmed by the absence of a capillary condensation step in the region of p/p_0 = 0.2–0.6. The decrease in mesoscopic ordering with increasing pre-hydrolysis time (Fig. 2) suggests that formation of Al–PMOs is hampered once pre-hydrolysis time exceeds 60 minutes. These reductions are at their greatest after 60 minutes of pre-hydrolysis under separate conditions (for example, for S-PMO-5-60-Y/Al SBET = 181 m^2g^{-1}). The increased amounts of residual template in the extracted Al-PMOs (confirmed by ^1H-^{13}C CP/MAS NMR, Fig. S3) compared with the Al-free PMO would cause such reductions in porosity. The reduced pore diameters may also be accounted for by the incorporation of more template into the as-synthesised Al-PMOs (confirmed by ^1H-^{13}C CP/MAS kinetics).

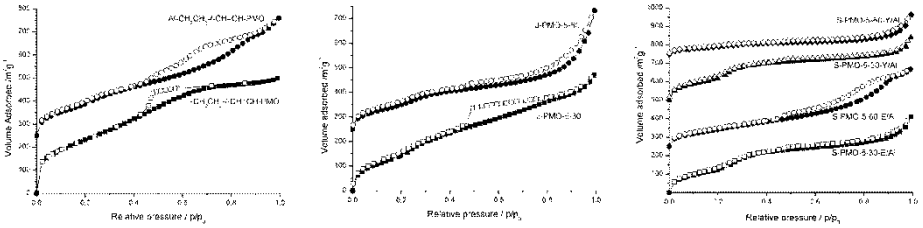

Fig. 3. N_2 sorption/ desorption isotherms (Top) and Pore size distribution plots (Bottom) recorded at 77 K for all PMOs.

Local structure of Al/–CH=CH–/CH_2–CH_2–PMO

Composition of reference PMOs

A typical ^{1}H-^{13}C CP/MAS NMR spectrum for as-synthesised PMO (Fig. 4, top) shows several resonances between 23.5 to 67.3 ppm attributed to the template (a full assignment is given in the figure). The aliphatic chain's end methyl group is rarely observed in CP spectra recorded using short contact times due to its high mobility. The broad peaks at ca. 5 and 146 ppm correspond to –CH_2–CH_2– and –CH=CH– functionalities respectively and confirm their incorporation into both mesostructures. The spectrum of the Al–CH_2CH_2–/–CH=CH–PMO shows evidence of small amount of template species even after three extractions, although the corresponding relative intensities are reduced. Despite this the material is still mesoporous and further extraction procedures would lead to complete dealumination and collapse of the framework.

The application of ^{1}H-^{13}C CP/MAS kinetics (Fig. 5) to the as-synthesised standard PMOs confirmed a higher content of the template for the aluminium containing analogue. Integration of the spectra recorded at 2 ms revealed the template content to be 3 times higher for the Al–/–CH_2CH_2–/–CH=CH–PMO compared to the –CH_2CH_2–/–CH=CH–PMO. Integration of the ^{1}H-^{13}C CP/MAS spectra of the Al–/–CH_2CH_2–/–CH=CH–PMO after three acid extractions showed a template content of 8.6 % with respect to the as-synthesised product. No evidence of template was seen in the Al-free PMO.

^{1}H-^{29}Si CP/MAS NMR spectrum of the –CH_2CH_2–/–CH=CH–PMO (Fig. 5, bottom) shows three intense resonances at ca. –56, –64 and –81 ppm corresponding to –CH_2–CH_2–Si $T^{2/3}$ sites (–CH_2–CH_2–$Si(OSi)_2(OH)$ and –CH_2–CH_2–$Si(OSi)_3$) respectively, whilst the peak at –81 ppm corresponds to a fully condensed silicon CH=CH– T^3 site (–CH=CH–$Si(OSi)_3$). A partially condensed silicon –CH=CH– T^2 environment is also present as a shoulder at *ca.* –71 ppm off the silicon –CH_2–CH_2– T^3 site resonance. The low-intensity peak at *ca.* –49 ppm corresponds to a poorly condensed silicon –CH_2–CH_2– T^1 site (CH_2–CH_2–$Si(OSi)(OH)_2$). The absence of any resonances in the region of –90 to –120 ppm corresponding to silicon Q^n sites indicates no Si–C bond cleavage has occurred during synthesis or template extraction.

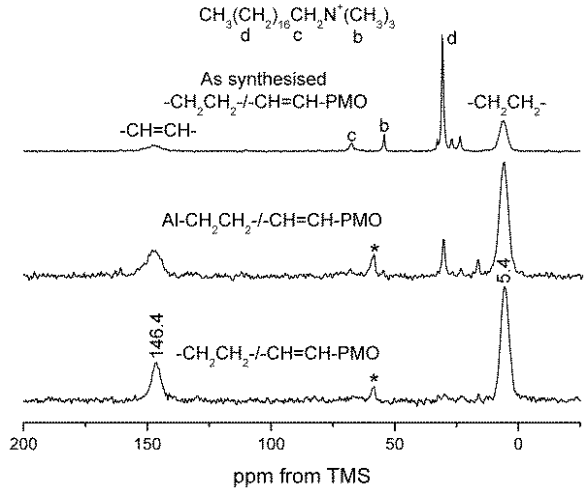

Fig. 4. ^{1}H-^{13}C CP/MAS NMR spectra of the as synthesised (Top) and template extracted reference PMOs.

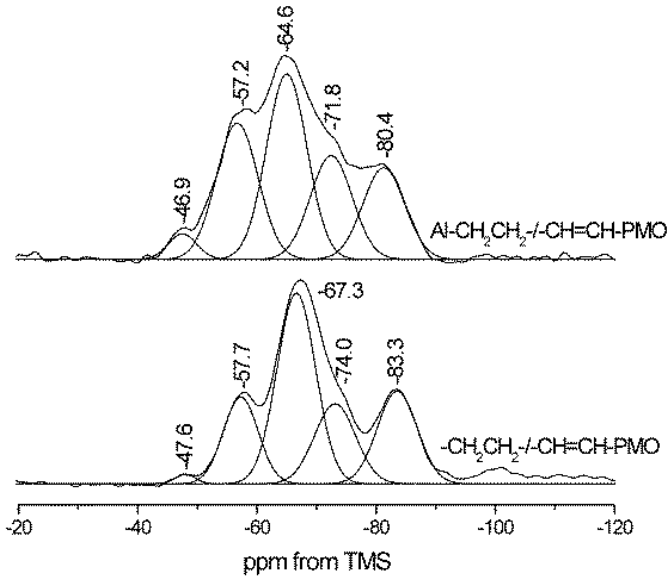

Fig. 5. ^{1}H-^{29}Si CP/MAS NMR spectra of the template extracted reference PMOs.

The introduction of Al into the framework resulted in a shift of both –CH_2CH_2– and –CH=CH–Si T^3 environments to higher ppm (Fig. 5, top). This confirms the shielding effect of the aluminium on the chemical shift of ^{29}Si nuclei similar to that observed in zeolites. The increase in peak area for the lines at both –64 and 71 ppm is a result of spectral overlap of T^2 silicon Al free and T^3 R–Si(OSi)$_2$(OAl) Al containing sites.

^{1}H-^{29}Si CP/MAS kinetics of the reference PMOs (Fig. 4 and table 2) indicate changes in $T_{1\rho}{}^H$ times as a consequence of incorporation of aluminium. The decrease in the $T_{1\rho}{}^H$ times for all silicon $T^{2/3}$ sites confirms aluminium is embedded in the pore walls and present on the pore wall interface. The influence of residual template in Al–PMOs on $T_{1\rho}{}^H$ times can be ignored as relaxation times for the T^3 sites (located away from the template in bulk pore wall) are also reduced. This change is a result of a ^{1}H/^{27}Al/^{29}Si dipolar coupled system where relaxation in the rotating frame is facilitated by the quadrupolar (I = 5/2) aluminium nucleus. For both organic bridges, the silicon T^2 sites always show faster CP build up than their respective T^3 environments due to the presence of Si–OH groups in T^2 and not in T^3 sites. The incorporation of aluminium has no effect on the TIS times because aluminium does not affect the ^{1}H-^{29}Si heteronuclear dipolar coupling.

Composition of the pre-hydrolysed Al–PMOs

^{1}H-^{13}C CP/MAS NMR spectra of the pre-hydrolysed Al–PMOs show the presence of both –CH_2CH_2– and –CH=CH– bridges at *ca.* 5 and 146 ppm respectively. The repeated extraction removed a large amount of the organic template although residual amounts remain as seen by the resonance at ca. 30 ppm as seen for the reference Al–PMO. The use of alternative extraction protocols, *i.e.* 50/50 v/v Acetic acid/ ethanol mixtures did remove the entire organic template in Al–CH_2CH_2–PMO without Al leaching. However, when this procedure was applied for the Al/–CH_2CH_2–/–CH=CH–PMOs the template remained in the pores, suggesting the CH=CH– bridge induces an increase in template framework interactions from an Al–CH_2CH_2–PMO. 1H-13C CP/MAS NMR spectra of the separately pre-hydrolysed Al-PMOs after three extractions show a reduction in template content compared to the J-PMOs.

^{1}H-^{29}Si CP/MAS NMR spectra of the pre-hydrolysed Al–PMOs display an increase in relative intensity of both CH_2CH_2– and –CH=CH–T^2 sites at *ca.* 57.2 and 71.8 ppm compared to the corresponding T^3 sites. This observation is a further confirmation that Al containing silicon T^3 sites resonate at the same frequency as the Al free silicon T^2 environments.

^{1}H-^{29}Si CP/MAS kinetics of the jointly pre-hydrolysed PMOs is similar to that of the reference Al–PMO. Although, the relative intensity of the –CH=CH–Si $T^{2/3}$ sites is increased compared to the –CH_2CH_2– environments with increasing pre-hydrolysis time. ^{1}H–^{29}Si CP/MAS kinetics of the separately pre hydrolysed PMOs highlight changes in the $T_{1\rho}{}^H$ times depending on the silicon precursor/Al(O^{i}C^{3}H^7)^3 combination during pre-hydrolysis. The E/Al-PMOs exhibit a very homogeneous structure as $T_{1\rho}{}^H$ times for all T sites are similar irrespective of pre-hydrolysis time. The intensity of the peaks of –CH=CH– T sites is increasingly similar to those of –CH_2CH_2– T sites with increasing pre-hydrolysis time. This is consistent with the analysis of the ^{29}Si CP/MAS NMR data which suggested a higher –CH=CH– content in comparison to the S-PMO-5-30/60 Y/Al. The Y/Al-PMOs displayed faster $T_{1\rho}{}^H$ times than the E/Al-PMOs. This indicates an increased Al content, confirmed by ^{27}Al MAS NMR (Fig 7), affects the $T_{1\rho}{}^H$ times of the framework. $T_{1\rho}{}^H$ times are also decreased as pre-hydrolysis time increases for both S-

PMO-5-30/60 E/Al and S-PMO-5-30/60 Y/Al which is consistent with increasing Al content (Fig. 7). The faster $T1\rho^H$ times with increasing Al content are a further proof to the presence of a three spin coupled system of $^1H/^{27}Al/^{29}Si$ whereby ^{27}Al facilitates relaxation. The T_{IS} times of the various T sites followed the same trends as seen for the standard PMOs.

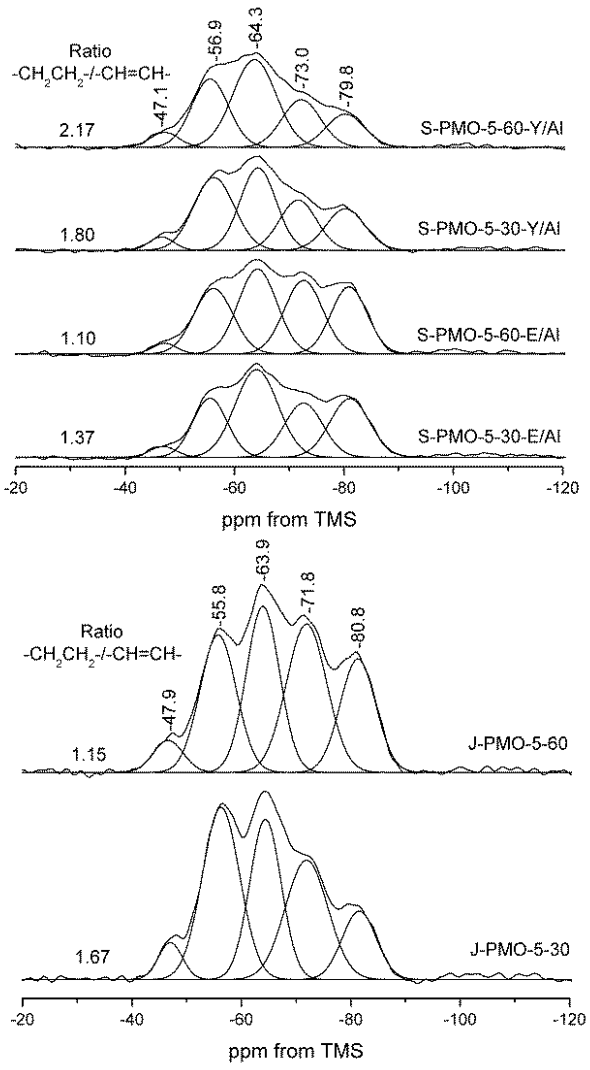

Fig. 6. ^1H-^{29}Si CP/MAS spectra of the joint and separately pre-hydrolysed Al containing PMOs after template extraction.

^{27}Al MAS NMR (Fig. 7) provided quantitative information on the aluminium content in the PMOs. The quantitative measurement of relative content of Al was ensured by conducting the ^{27}Al MAS NMR experiments using exactly the same sample volume and experimental conditions (number of scans, recycle delay etc.). The ^{27}Al MAS NMR spectra show resonances at 55 and 0 ppm corresponding to aluminium in tetrahedral and octahedral environments. The aluminium content of the PMOs is increased with pre-hydrolysis time for both J- and S-PMOs (determined from a Gaussian deconvolution of the Al [4] resonance). ^{27}Al CP/MAS NMR spectra are similar to ^{27}Al MAS NMR spectra, however, the Al [6] environments have increased intensity *c.f.* Al [4] sites.

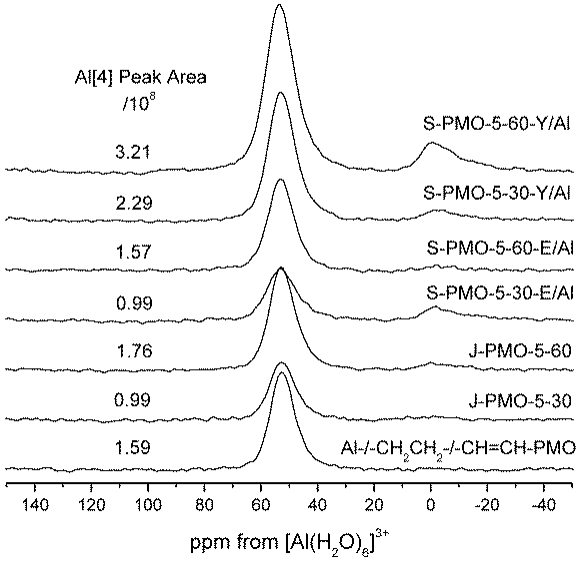

Fig. 7. ^{27}Al MAS NMR spectra of aluminium containing PMOs after template extraction.

Distribution of functional groups ^{1}H-^{29}Si HETCOR experiments.

2D ^{1}H-^{29}Si HETCOR experiments were used to probe the spatial proximity of the organic functionalities in the framework. The same $T^{2}/^{3}$ sites as those in the 1D ^{1}H-^{29}Si CP/MAS (Figs. 5 and 6) in the direct dimension are correlated to the FSLG decoupled ^{1}H MAS spectrum in the indirect dimension.

The ^{1}H-^{29}Si HETCOR spectra of the reference –CH_2CH_2–/–CH=CH–PMO and Al–/–CH_2CH_2–/–CH=CH–PMO are shown in figure 8. The ^{1}H dimension exhibits four/five resonances. The resonances at 0.8 and 4.2 ppm are assigned to surface hydroxyls (silanol groups) and H-bonded water located within the pore walls, close to the silicon $T^{2,3}$ sites. The peak at 1.8 ppm is attributed to the –CH_2–CH_2– protons with auto-peaks observed in the ^{29}Si direct dimension at –56.6 and –63.9 ppm correlating to ≡Si–CH_2–CH_2–Si≡ $T^{2,3}$ environments. The peak at 6.8 ppm is assigned to the –CH=CH– protons with auto-peaks observed in the ^{29}Si dimension at –72.0 and –82.2 ppm indicative of ≡Si–CH–CH–Si≡

$T^{2,3}$ sites. In addition, cross-peaks correlating the $–CH_2–CH_2–$ bridge ^1H resonance to the –CH=CH– silicon $T^{2,3}$ sites and vice versa are observed. The $^1H–^{29}Si$ HETCOR spectrum of the reference Al–PMO (Fig. 8b) shows an increase in the –CH=CH– auto-peak intensity relative to the $–CH_2CH_2–$ sites compared to the $–CH_2CH_2–$/–CH=CH– PMO.

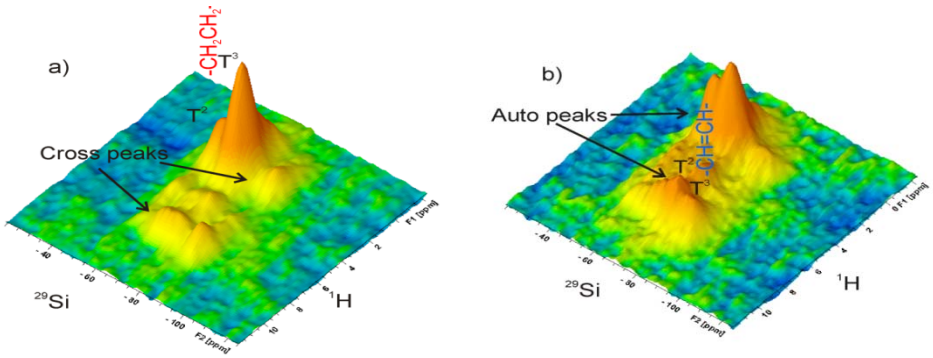

Fig. 8. ^1H-^{29}Si HETCOR NMR spectra of
a) $–CH_2CH_2–$/–CH=CH–PMO and
b) Al–CH_2CH_2 /–CH=CH–PMO after template extraction.

The degree of heterogeneity can be estimated using intensities of $–CH_2–CH_2–$ and –CH=CH– ^1H-^{29}Si correlations from the 2-dimensional data set. High auto peak/cross peak ratios indicate a heterogeneous domain type distribution whereas lower values suggest a more homogenous framework. The analogous acid catalysed $CH_2CH_2–$/–CH=CH–PMOs showed a distinct difference in ^1H-^{29}Si correlation intensities as a function of pre-hydrolysis protocols whereby, J–PMOs displayed homogeneous structures and S–PMOs displayed heterogeneous structures. In the S^+I^- systems the distribution of organic functionalities is less homogeneous than in the acid catalysed J–PMOs, however, more homogeneous than in the acid catalysed S–PMOs [22]. Therefore the S^+I^- $–CH_2CH_2–$/–CH=CH–PMOs have an intermediate structure were domains exist but are smaller and/or less segregated. The homogeneity of Al/$–CH_2CH_2–$/–CH=CH–PMO is increased compared to the Al free analogue with an increase in cross-peak intensities of both organic functionalities. This confirms aluminium to affect the co-assembly and formation of the mesostructure during synthesis as was observed using powder XRD.

^1H-^{27}Al HETCOR experiments

^1H-^{27}Al HETCOR experiments were used to study the distribution of aluminium in the mesoporous framework. The application of ^1H-^{27}Al HETCOR experiments has been limited to the study of zeolites, Al doped mesoporous silicas and clays. This is in part due to the poor resolution in both ^1H and ^{27}Al dimensions resulting from homonuclear dipolar coupling and quadrupolar interactions. The ^1H-^{27}Al HETCOR NMR spectra of Al/$–CH_2CH_2–$/–CH=CH–PMO and S-PMO-5-30-E/Al (Fig. 9a and b respectively) correlates the 1D ^{27}Al CP/MAS spectrum in f_2 to the FSLG decoupled ^1H MAS NMR spectrum in the f_1 dimension. The ^1H dimension exhibits three resonances. The

resonance at 4.2 ppm is assigned to acidic protons and adsorbed water with correlation peaks to the ^{27}Al resonances at *ca.* 53 and 0 ppm attributed to framework aluminium ($Al(O)_4$) and octahedrally bound $Al[(H_2O)_6]^{3+}$ species respectively. ^{1}H resonances at 1.8 and 6.8 ppm are due to –CH_2–CH_2– and –CH=CH– protons with correlations observed in the ^{27}Al direct dimension at 52.9 ppm confirming assignment as framework aluminium. No cross-peaks correlating the organic bridges and $Al[(H_2O)_6]^{3+}$ are observed. Therefore, the latter species are located at the surface of the pores. Both the reference Al-PMO and S-PMO-5-30-E/Al show near identical cross-peaks with a small increase in –CH=CH–/Al [4] correlation intensity for the latter. This confirms aluminium is not located preferentially to a specific organic bridge when using separate pre-hydrolysis protocols. Therefore the aluminium must re-disperse in the synthesis solution during the low and/or high temperature steps after pre-hydrolysis to be evenly distributed in the framework.

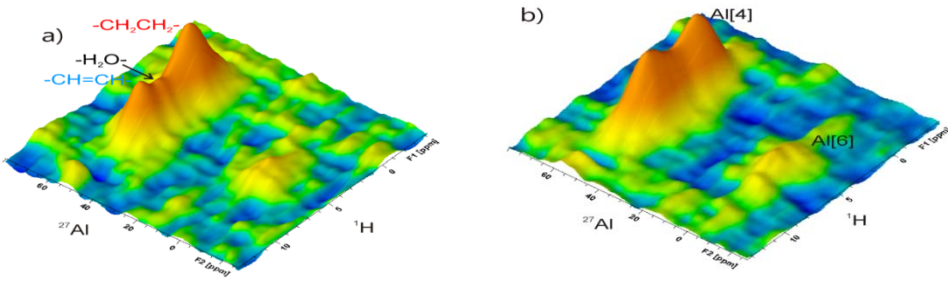

Fig. 9. ^{1}H-^{27}Al HETCOR spectra of
a) Al-CH_2CH_2-/-CH=CH-PMO and
b) S-PMO-5-30-E/Al after template extraction.

Conclusions

Periodic mesoporous organosilicas containing –CH_2–CH_2–/–CH=CH– and –Al–/–CH_2–CH_2–/–CH=CH– functionalities have been synthesised. Joint and separate pre-hydrolysis protocols were employed in an attempt to control the distribution of the organic and aluminium functionalities into homogeneous and heterogeneous domains.

The introduction of aluminium into the –CH_2CH_2–/–CH=CH–PMO resulted in an increase in mesoscopic ordering the origin of which is the negatively charged Al [4] centres within the framework. The presence of negatively charged aluminium sites resulted in an increase in template content in the as-synthesised Al-PMOs compared to the Al free analogues. The use of Aluminium as a probe enabled further investigation into the influence of Joint and separate Pre-hydrolysis protocols on Al–/–CH_2CH_2–/–CH=CH–PMOs. Aluminium was re-dispersing in the reaction media after the pre-hydrolysis was complete. Re-dispersion may not be isolated to aluminium and it is also possible that the –CH_2CH_2– and –CH=CH– containing SBUs also partially re-disperse during the synthesis. This hypothesis is consistent with the conclusions of Lowe *et al.* on zeolite formation (Scheme 1). This result highlights both the difficulty in predicting the distribution of multi component porous materials with localised functionality domains in the same porous structure.

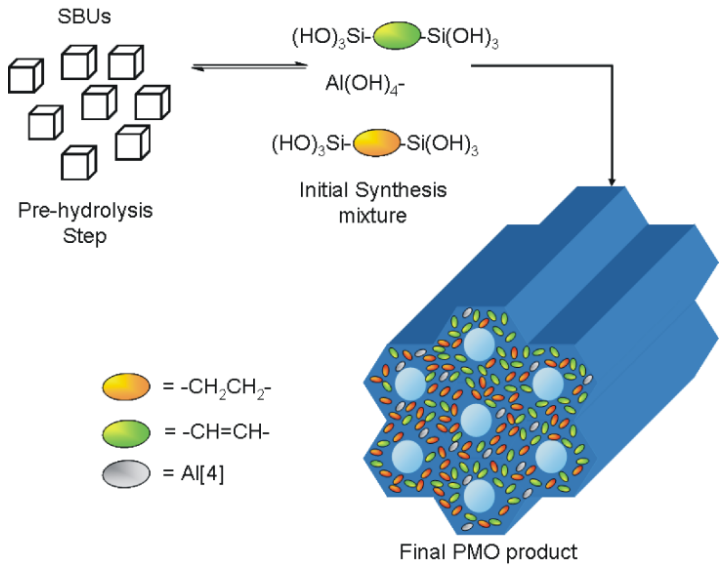

Scheme 1. Proposed re-dispersion of SBUs upon addition to the template solution as indicated by solid-state NMR.

LITERATURE

1. *Asefa T., MacLachlan M. J., Coombs N. and Ozin G. A.* Periodic mesoporous organosilicas with organic groups inside the channel walls // Nature. – 1999. – Vol. 402. – P. 867–871. doi:10.1038/47229
2. *Yoshina-Ishii C., Asefa T., Coombs N., MacLachlan M. J. and Ozin G. A.* Periodic mesoporous organosilicas, PMOs: fusion of organic and inorganic chemistry ‘inside’ the channel walls of hexagonal mesoporous silica // Chemical Communications. – 1999. – P. 2539–2540. doi:10.1039/a908252b
3. *Asefa T., Coombs N., Dag O., Yoshina-Ishii C., MacLachlan M.J., Ozin G.A.* Periodic mesoporous organosilicas (PMOs) with functional organic groups inside the channel walls. Abstracts of Papers of the American Chemical Society. – 2000. – Vol. 219. – P. U883–U883.
4. *Asefa T., Yoshina-Ishii C., MacLachlan M. J.and Ozin G. A.* New nanocomposites: putting organic function "inside" the channel walls of periodic mesoporous silica // Journal of Materials Chemistry. – 2000. – Vol. 10. – P. 1751–1755. doi:10.1039/b000950o.
5. *Hatton B., Landskron K., Whitnall W., Perovic D., Ozin G. A.* Past, present, and future of periodic mesoporous organosilicas-the PMOs // Accounts of Chemical Research. – 2005. – Vol. 38. – P. 305–312. doi:10.1021/ar040164a.
6. *Hunks W. J. and Ozin G. A.* Challenges and advances in the chemistry of periodic mesoporous organosilicas (PMOs) // Journal of Materials Chemistry. – 2005. – Vol. 15. – P. 3716–3724. doi:10.1039/b504511h.
7. *Hoffmann F., Cornelius M., Morell J., Froba M.* Periodic Mesoporous Organosilicas (PMOs): Past, Present, and Future // Journal of Nanoscience and Nanotechnology. – 2006. – Vol. 6. – P. 265–288. doi:10.1166/jnn.2006.902.

8. *Yang Q.-H., Liu J., Zhong H., Wang P.-Y.* Progress in the periodic mesoporous organosilicas // Journal of Inorganic Materials. – 2009. – Vol. 24. – P. 641–649.
9. *Chu C. T. W., Chang C. D.* Journal of Physical Chemistry. – 1985. – Vol. 89. – P. 1569–1571.
10. *Guo W. P., Zhao X. S.* Microporous and Mesoporous Materials. – 2005. – Vol. 85. – P. 32–38.
11. *Hughes B. J., Guilbaud J. B., Allix M., Khimyak Y. Z.* Journal of Materials Chemistry. – 2005. – Vol. 15. – P. 4728–4733.
12. *Hoffmann F., Cornelius M., Morell J., Froeba M.* Silica-Based Mesoporous Organic–Inorganic Hybrid Materials // Angewandte Chemie-International Edition – 2006. – Vol. 45. – P. 3216–3251. doi:10.1002/anie.200503075.
13. *Cho W., Park J. W., Ha C. S.* Materials Letters. – 2004. – Vol. 58. – P. 3551–3554.
14. *Kapoor M. P., Bhaumik A., Inagaki S., Kuraoka K., Yazawa T.* Titanium containing inorganic-organic hybrid mesoporous materials with exceptional activity in epoxidation of alkenes using hydrogen peroxide // Journal of Materials Chemistry. – 2002. – Vol. 12. – P. 3078–3083. doi:10.1039/b204524a.
15. *Shylesh S., Srilakshmi C., Singh A. P., Anderson B. G.* One step synthesis of chromium-containing periodic mesoporous organosilicas and their catalytic activity in the oxidation of cyclohexane // Microporous and Mesoporous Materials. – 2007. – Vol. 99. – P. 334–344. doi:10.1016/j.micromeso.2006.09.029.
16. *Shylesh S., Singh A. P.* Vanadium-containing ethane–silica hybrid periodic mesoporous organosilicas: Synthesis, structural characterization and catalytic applications // Microporous and Mesoporous Materials. – 2006. – Vol. 94. – P. 127–138. doi:10.1016/j.micromeso.2006.03.027.
17. *Tobyn M., Brown J., Dennis A. B., Fakes M., Gao Q., Gamble J., Khimyak Y. Z., McGeorge G., Patel C., Sinclair W., Timmins P., Yin S.* Amorphous drug-PVP dispersions: Application of theoretical, thermal and spectroscopic analytical techniques to the study of a molecule with intermolecular bonds in both the crystalline and pure amorphous state // Journal of Pharmaceutical Sciences. – 2009. – Vol. 98. – P. 3456–3468. doi:10/1002/jps.21738.
18. *Jiang J.-X., Su F., Trewin A., Wood C. D., Campbell N. L., Niu H., Dickinson C., Ganin A. Y., Rosseinsky M. J., Khimyak Y. Z., Cooper A. I.* Conjugated Microporous Poly(aryleneethynylene) Networks // Angewandte Chemie-International Edition. – 2007. – Vol. 46. – P. 8574–8578. doi:10.1002/anie.200701595.
19. *Khimyak Y. Z., Klinowski J.* Solid-state NMR studies of the organic template in mesostructured Aluminophosphates // Physical Chemistry Chemical Physics. – 2001. – Vol. 3. P. 616–626. doi:10.1039/b007473j.
20. *Vercaemst C., Ide M., Wiper P. V., Jones J. T. A., Khimyak Y. Z., Verpoort F., Van Der Voort P.* Ethenylene-Bridged Periodic Mesoporous Organosilicas: From E to Z // Chemistry of Materials. – 2009. – Vol. 21. – P. 5792–5800. doi:10.1021/cm902164t.
21. *Vercaemst C., Jones J. T. A., Khimyak Y. Z., Martins J. C., Verpoort F., Van der Voort P.* Spectroscopic evidence of thermally induced metamorphosis in ethenylene-bridged periodic mesoporous organosilicas // Physical Chemistry Chemical Physics. – 2008. – Vol. 10. P. 5349–5352. doi:10.1039/b808630n
22. *Jones J. T. A., Wood C. D., Dickinson C. Khimyak Y. Z.* Periodic Mesoporous Organosilicas with Domain Functionality: Synthesis and Advanced Characterization // Chemistry of Materials. – 2008. – Vol. 20. – P. 3385–3397. doi:10.1021/cm7036124.
23. *States D. J. H., Ruben R. A., D. J.* J. Magn. Reson., A Two-Dimensional Nuclear Overhauser Experiment with Pure Absorption Phase in Four Quadrants // Journal of Magnetic Resonance Ser. A. – 1982. – Vol. 48. – P. 286–292. doi:10.1016/0022-2364(82)90279-7.
24. *Keeler J. N., D. J.* J. Magn. Reson. – Ser. A. – 1985. – Vol. 63.
25. *Jones J. T. A.* PhD Thesis Synthesis and Characterization of Porous Organic/Inorganic Hybrid Materials,", University of Liverpool, Liverpool, 2009. – p. 273.

РЕЗЮМЕ

Д. Т. А. ДЖОНС[1], П. В. ВАЙПЕР[1], Я. З. ХІМ'ЯК[1,2]

ВКЛЮЧЕННЯ АЛЮМІНІЮ В –CH_2–CH_2–/–CH=CH–ПМО

[1]Хімічний факультет Ліверпульського університету,
Ліверпуль, Великобританія

[2]Школа фармації, Університет Східної Англії,
Норвіч, Великобританія
e-mail: Y.Khimyak@uea.ac.uk

Періодичні мезопористі органосилікати (ПМО), які містять –CH_2–CH_2–/–CH=CH– та –Al–/–CH_2–CH_2–/–CH=CH– функціональні групи, було синтезовано, використовуючи спосіб поєднаного або роздільного перед-гідролізу для контролю розподілу органічних функціональних груп та алюмінію в гомогенних або гетерогенних доменах.

Додавання алюмінію в –CH_2–CH_2–/–CH=CH–ПМО привело до збільшення впорядкування на рівні мезопор. Це пов'язано з присутністю негативно заряджених Al(4) центрів в структурі. Ці центри зумовлюють збільшення вмісту органічних структурованих частинок у синтезованих –Al–/–CH_2–CH_2–/–CH=CH– ПМО у порівнянні з –CH_2–CH_2–/–CH=CH–ПМО.

Використання алюмінію як індикатора впорядкування, дозволило дослідити механізм способів поєднаного або роздільного перед-гідролізу на прикладі –Al–/–CH_2–CH_2–/–CH=CH–ПМО. Використання ^{27}Al, ^{29}Si, ^{13}C, ^{1}H ЯМР в твердому стані дозволило дослідити деталі структури на молекулярному рівні та підтвердити запропонований механізм розподілу різних функціональних груп в стінках пор для матеріалів, одержаних різними синтетичними протоколами.

Алюміній має можливість бути розчиненим в реакційному середовищі після закінчення перед-гідролізу. Такий перерозподіл є властивий не лише алюмінію, але й вторинним структурним частинкам, які містять –CH_2–CH_2– та –CH=CH– функціональні групи. Ці результати погоджуються з відомими механізмами формування мікропористих цеолітів, а також вказують на труднощі, пов'язані з передбаченням розподілу різних функціональних груп у багатокомпонентних пористих матеріалах.

Ключові слова: алюміній, мезопористі органосилікати.

Стаття надійшла 29.08.2018.
Після доопрацювання : 22.09.2018.
Прийнята до друку 28.09.2018.